TRANSACTIONS
OF TIANJIN UNIVERSITY

2016, 22: 473-479
DOI 10.1007/s12209-016-2776-x

Characterization and Photocatalytic Activity of Mixed Nanocrystalline TiO_2 Powders Prepared by Xerogel-Hydrothermal Method in Different Acid Solutions*

Liu Cuiping (刘翠萍)[1, 2], Yu Tao (于 涛)[1], Tan Xin (谭 欣)[3]

(1. School of Chemical Engineering and Technology, Tianjin University, Tianjin 300072, China;
2. School of Science, Tianjin Chengjian University, Tianjin 300384, China;
3. School of Science, Tibet University, Tibet 850000, China)

Abstract: TiO_2 nanoparticles (NPs) were prepared via the hydrothermal route of TiO_2 xerogel in nitric acid, hydrochloric acid and acetic acid. The physico-chemical properties of the powders were characterized by X-ray diffraction (XRD) and N_2 adsorption desorption techniques. The effects of the different acids on the structure (crystal phase) and texture (primary particle size and porosity) of the TiO_2 powders were explored. Results indicated that acetic acid facilitated the formation and stability of pure anatase phase. On the other hand, nitric acid and hydrochloric acid led to the transformation from anatase to rutile. The catalyst synthesized via the hydrothermal route of TiO_2 xerogel in the low concentration hydrochloric acid solution (Ti-HCl-0.15) had the highest photocatalytic activity than the catalysts obtained in the other two acid solutions. The effects of the different acids were discussed in terms of acid strength, chelating effect and the thermal stability of the adsorbed acidic anions.

Keywords: TiO_2 xerogel; hydrothermal; anatase

Since the discovery of photocatalytic properties in titania, it has attracted much attention because of its good catalytic properties, chemical inertness and stability, wide and tunable band gap, good transmittance as well as high fractive index, which make it useful for many environmental and electrical applications such as photocatalysts[1, 2], photovoltaics[3, 4], gassensors[5].

There were many investigative reports on TiO_2 sol and gel which were related to the preparation, characterization, modification, and application. Based on these reports, several methods were proposed for the preparation of TiO_2 sol and gel photocatalyst, such as colloidal TiO_2 nanoparticles (NPs) dispersion method[6], sol-gel-thermal method[7], and gel-peptization method[8, 9]. As for xerogel, TiO_2 NPs produced by the acid peptization of xerogel and the hydrothermal of xerogel in distilled water had been reported. Acid peptization process encouraged the dividing of large aggregated and/or agglomerated particles into small colloidal particles[10]. After hydrothermal treatment in distilled water, amorphous xerogel powders crystallized into anatase and the surface area of the powders increased significantly[11, 12].

However, TiO_2 synthesized via the hydrothermal route of TiO_2 xerogel in different acid solutions has not been reported. In this work, the xerogel was subjected to hydrothermal treatment in hydrochloric acid (HCl), acetic acid (CH_3COOH) and nitric acid (HNO_3) solutions with a certain concentration to promote the formation of NPs. The catalysts were characterized with X-ray diffraction (XRD), scanning electron microscope (SEM) and Brunauer Emmett Teller (BET) method. The influences of different acids on the crystallinity, absorption capacity of TiO_2 particles and its photodegradation performance for methyl blue (MB) were investigated in detail. Possible mechanism of anatase formed under hydrothermal condition was discussed.

Accepted date: 2015-12-18.
*Supported by the National Basic Research Program of China ("973" Program, No. 2014CB239300, No. 2012CB720100) and National Natural Science Foundation of China (No. 21406164, No. 21466035).
Liu Cuiping, born in 1977, female, lecturer.
Correspondence to Yu Tao, E-mail: yutao@tju.edu.cn.

1 Experimental

1.1 Catalyst preparation

The preparation of TiO_2 NPs involved the following steps. First, tetrabutyl titanate and ethanol were mixed and stirred for 30 min at room temperature (solution A). An appropriate amount of HNO_3 solution was dissolved in ethanol. Then, solution B was dropped into solution A under stirring for 2 h. Thereafter, the solution was aged until the gel formed. The colloid was first dried at 80 ℃ to form xerogel. The xerogel was added to HCl, CH_3COOH and HNO_3 solution respectively with different concentrations (0.15, 1.5, 3 mol/L). The final mixture was transferred into a Teflon-lined stainless steel autoclave, and then heated at 393 K for 12 h. The product was washed by water and ethanol several times and dried at 80 ℃. The samples obtained in HCl, HNO_3 and CH_3COOH solution were assigned as Ti-HCl-0.15, Ti-HCl-1.5, Ti-HCl-3; Ti-HNO_3-0.15, Ti-HNO_3-1.5, Ti-HNO_3-3; Ti-CH_3COOH-0.15, Ti-CH_3COOH-1.5, Ti-CH_3COOH-3, corresponding to different concentrations (0.15, 1.5, 3 mol/L) of HCl, HNO_3 and CH_3COOH solution.

1.2 Sample characterization

The phase compositions of samples were identified by XRD (Cu Kα radiation). The crystallite sizes of the composite catalysts were calculated using the Scherrer equation. For the samples, the weight fraction of every component can be calculated from

$$W_A = \frac{k_A A_A}{k_A A_A + A_R + k_B A_B}$$

$$W_B = \frac{k_B A_B}{k_A A_A + A_R + k_B A_B}$$

$$W_R = \frac{A_R}{k_A A_A + A_R + k_B A_B}$$

where W_A, W_B and W_R represent the weight fractions of anatase, brookite and rutile, respectively; coefficients k_A and k_B are 0.886 and 2.721, respectively; and A_A, A_B and A_R represent the integrated intensity of the anatase (101) peak ($2\theta = 25.28°$), the brookite (121) peak ($2\theta = 30.81°$), and the rutile (110) peak ($2\theta = 27.45°$), respectively. Because the brookite (120) ($2\theta = 25.34°$) and brookite (111) ($2\theta = 25.69°$) peaks overlap with the anatase (101) peak, A_A and A_B were calculated by the following method. The single isolated brookite (121) peak was used as a reference, the anatase (101), brookite (120) and brookite (111) overlapped peaks were deconvoluted by I(brookite 121)/I(brookite 120) = 0.9 and I(brookite 111)/I(brookite 120) = 0.8 [13].

The specific surface areas of the samples were deduced by BET method (N_2 adsorption) with a NOVA-2000E instrument. Nitrogen adsorption/desorption isotherms were measured at 196 ℃. Surface area (S_{BET}) was calculated by applying the BET equation [14]. Barrett Joyner Halenda (BJH) approach was used to calculate the pore size distribution of the samples using the desorption data. The morphologies of the samples were observed by field emission scanning electron microscope (FESEM, Hitachi S-6800).

1.3 Photodegradation of MB

The photocatalytic activity was monitored by the degradation rate of MB solutions. The photodegradation was carried out in 80 mL MB (10 mg/L) solution in the presence of catalyst under magnetic stirring and air bubbling. This mixture was magnetically stirred for 30 min to reach adsorption equilibrium in the darkness. Then, the mixture was placed 15 cm away from the light source of Xe lamps (HSX-F/UV300, Beijing Nbet Technology Co., Ltd). For comparison, a blank experiment for the system without catalyst was also conducted under the same condition. To prevent light leakage, the vessel and the light source were placed inside a black box. The experiments were conducted at room temperature.

2 Results and discussion

2.1 Characterization

2.1.1 XRD

XRD patterns for the as-prepared TiO_2 NPs are shown in Fig. 1. It can be observed that the synthesized Ti-HCl, Ti-HNO_3 and Ti-CH_3COOH show a mixed phase of TiO_2 anatase, brookite and rutile. When the concentrations of HCl, HNO_3 and CH_3COOH were 0.15 mol/L and 1.5 mol/L, all Ti-HCl, Ti-HNO_3 and Ti-CH_3COOH were a mixture containing a large amount of anatase and a small amount of brookite. However, with the concentrations of HCl, HNO_3 and CH_3COOH increasing, the content of brookite decreased and the content of rutile increased. The indexed crystal phase type and particle size calculated for each sample are listed in Tab. 1. As for Ti-HCl, Ti-HNO_3 and Ti-CH_3COOH, the size of anatase crystallites increased when the concentration was elevated to 3 mol/L. When both anatase and rutile are present, the

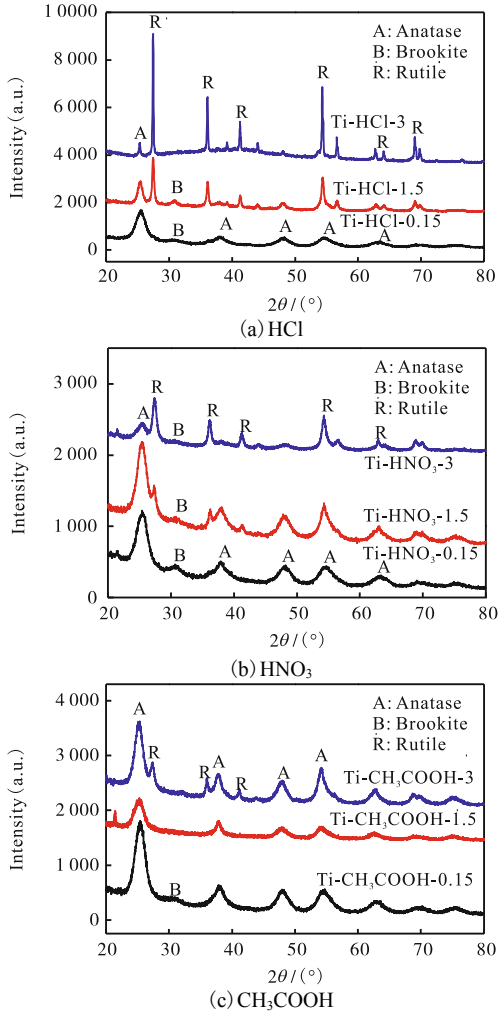

Fig. 1 XRD of the as-prepared samples with the hydrothermal treatment of titania xerogel in different acid solutions

size of anatase crystallite is invariably smaller than that of rutile. This result is similar to the work reported by Gopal *et al*[15], where they found that the size of anatase crystallite was smaller than that of rutile in the mixed sample. Similarly, when both anatase and brookite are present, the size of anatase crystallite is invariably smaller than that of brookite. The possible mechanism for the formation of anatase, brookite and rutile will be discussed in Section 2.3.

2.1.2 Analyses of SEM

To obtain the information about the morphology of Ti-HCl-1.5, Ti-HNO_3-1.5 and Ti-CH_3COOH-1.5, some selected powders were investigated by SEM, as shown in Fig. 2. Fig. 2 (a) shows a rod-like mixed phase (anatase, rutile and brookite) formed in hydrochloric acid. It can be observed from Fig. 2 (b) that some small quasi-spherical particles are aggregated on the surface of the rod-like particles in the presence of HNO_3. The samples shown in Fig. 2 (a) and Fig. 2 (b) are Ti-HCl-1.5 (35.3% anatase and 40.5% rutile and 24.2% brookite) and Ti-HNO_3-1.5 (91.2% anatase and 5.9% rutile and 2.9% brookite), respectively. Since the content of rutile in Ti-HCl-1.5 was higher than that in Ti-HNO_3-1.5, the rod-like particles in Ti-HCl-1.5 are more than those in Ti-HNO_3-1.5. Fig. 2 (c) shows that Ti-CH_3COOH-1.5 (100% anatase) was aggregated by small quasi-spherical particles.

Tab. 1 Comparison of the as-prepared samples in different acid solutions

Sample	Anatase		Rutile		Brookite	
	Phase type/%	Particle size/nm	Phase type/%	Particle size/nm	Phase type/%	Particle size/nm
Ti-HCl-0.15	85.2	4.7	0	0	14.8	7.0
Ti-HCl-1.5	35.3	11.2	40.5	21.5	24.2	8.6
Ti-HCl-3	13.5	15.6	86.5	31.6	0	0
Ti-HNO_3-0.15	80.1	4.7	0	0	19.9	6.3
Ti-HNO_3-1.5	91.2	6.3	5.9	18.5	2.9	8.5
Ti-HNO_3-3	26.8	7.8	66.3	12.8	6.9	10.7
Ti-CH_3COOH-0.15	98.9	4.9	0	0	1.1	8.3
Ti-CH_3COOH-1.5	100	4.9	0	0	0	0
Ti-CH_3COOH-3	86	6.7	14	15.2	0	0

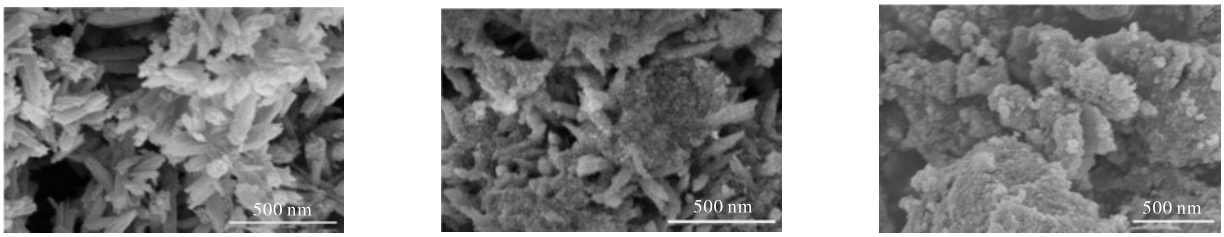

(a) Ti-HCl-1.5 (b) Ti-HNO_3-1.5 (c) Ti-CH_3COOH-1.5

Fig. 2 SEM images of Ti-HCl-1.5, Ti-HNO_3-1.5 and Ti-CH_3COOH-1.5

2.1.3 BET

Nitrogen adsorption/desorption isotherms for the catalysts synthesized via hydrothermal route of titania xerogel in hydrochloric acid solution are shown in Fig. 3(a). The isotherms of Ti-HCl-0.15 and Ti-HCl-1.5 can be categorized as type Ⅳ with an H2 hysteresis loop. While the isotherm of Ti-HCl-3 exhibits a type II sorption behavior without the existence of hysteresis loop, as shown in Fig. 3(a), indicating the presence of macropores according to the classification of IUPAC[16]. This indicates the change of porosity from micropores to macropores with the concentration of HCl increasing. As shown in Fig. 3(c), type Ⅳ isotherms with an H3 hysteresis loop are observed for Ti-HNO_3-0.15 and Ti-HNO_3-3, while type Ⅱ isotherm with an H2 hysteresis loop is assigned to Ti-HNO_3-1.5. From Fig. 3(e), type Ⅳ isotherms are observed for Ti-CH_3COOH-0.15 and Ti-CH_3COOH-3, while type Ⅱ isotherm is assigned to Ti-CH_3COOH-1.5. H2, H1 and H3 hysteresis loops are assigned to Ti-CH_3COOH-0.15, Ti-CH_3COOH-3 and Ti-CH_3COOH-1.5, respectively[16]. Fig. 3(b), (d) and (f) show that the pore size distributions of Ti-HCl, Ti-HNO_3 and Ti-CH_3COOH ranged from 5 to 15 nm except Ti-HCl-3, which is compatible with the observation from HRTEM (Fig. 4(b)).

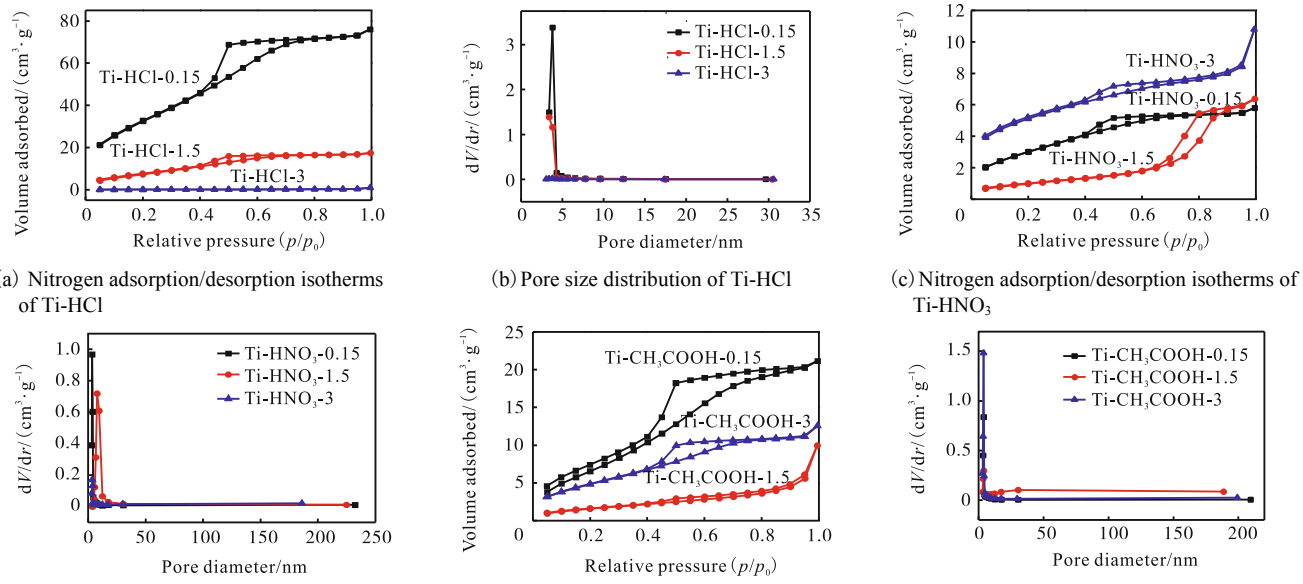

(a) Nitrogen adsorption/desorption isotherms of Ti-HCl

(b) Pore size distribution of Ti-HCl

(c) Nitrogen adsorption/desorption isotherms of Ti-HNO_3

(d) Pore size distribution of Ti-HNO_3

(e) Nitrogen adsorption/desorption isotherms of Ti-CH_3COOH

(f) Pore size distribution of Ti-CH_3COOH

Fig. 3 Nitrogen adsorption/desorption TiO_2 synthesized in different acid solutions

Tab. 2 shows the BET surface area, pore volume and pore diameter of the as-synthesized samples. As the concentrations of HCl and HNO_3 increase from 0.15 mol/L to 3 mol/L, the specific surface area and pore volume decrease, whereas the mean pore diameter changes irregularly. This is related to the transformation of the morphology, probably due to the growth of the nanocrystallites inside the pores. Some large nanocrystals of TiO_2 can be thrusted into the channels and block the mesopores which mainly resulted from the hydrothermal treatment in strong acid solution[17]. However, with the concentration of CH_3COOH increasing from 0.15 mol/L to 3 mol/L, the specific surface area and pore volume increase, but the mean pore diameter is almost unchanged. The increase of specific surface area and pore volume may be attributed to the generation of a plenty of micropores in the frameworks

Tab. 2 Textural characteristics of the as-prepared samples in different acid solutions

Sample	Pore volume/($cm^3 \cdot g^{-1}$)	S_{BET}/($m^2 \cdot g^{-1}$)	Mean pore diameter/nm
Ti-HCl-0.15	0.146	237.7	3.41
Ti-HCl-1.5	0.077	138.4	3.43
Ti-HCl-3	0.015	3.1	3.06
Ti-HNO_3-0.15	0.113	250.4	3.06
Ti-HNO_3-1.5	0.170	64. 9	9.59
Ti-HNO_3-3	0.052	99.6	3.06
Ti-CH_3COOH-0.15	0.082	75.5	3.07
Ti-CH_3COOH-1.5	0.177	77.3	3.05
Ti-CH_3COOH-3	0.161	201.2	3.05

which mainly resulted from the hydrothermal treatment in weak acid solution[18].

2.1.4 TEM

Fig. 4(a) shows the TEM image of Ti-HCl-0.15 which is pure anatase with the spheroidal-shaped morphology, and the average size of anatase crystallite is 6—10 nm. The difference of the particle size estimated by TEM and XRD is attributed to the particle agglomeration. The spacing of 0.371 nm corresponding to the (101) plane of anatase can be observed in Fig. 4(b), indicating the presence of anatase with the typical (101) direction. The TEM results confirmed that when the concentration of HCl was 0.15 mol/L, Ti-HCl-0.15 was a main anatase.

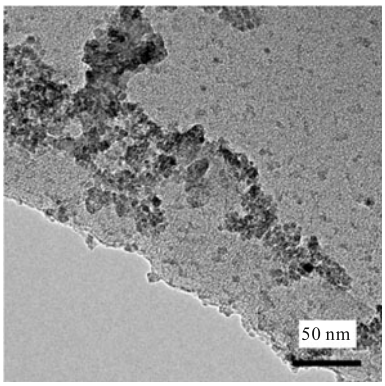

(a) TEM image

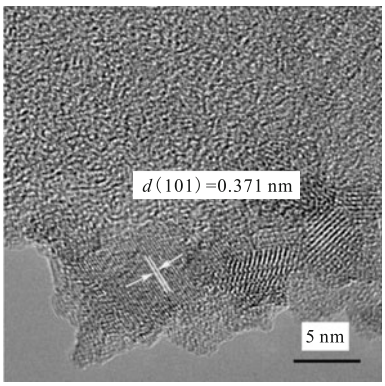

(b) HRTEM image

Fig. 4 TEM and HRTEM images of Ti-HCl-0.15

2.1.5 Optical property

Fig. 5 shows the UV-Vis diffuse reflectance spectra of Ti-HCl-0.15, Ti-HNO_3-0.15 and Ti-CH_3COOH-0.15. As shown in Fig. 5, with the proportion of anatase in the mixed-phase samples increasing, the absorption edge gradually shifts from 380 to 400 nm. The band gap (E_g) can be estimated by Kubelka-Munk function. As shown in Fig. 5, the E_g values show a slight decrease in the order of Ti-HCl-0.15, Ti-HNO_3-0.15 and Ti-CH_3COOH-0.15, indicating that the content of brookite in the samples would influence the indirect band gap value of TiO_2. Moreover, the light absorption of Ti-HNO_3-0.15 and Ti-CH_3COOH-0.15 is lower than that of Ti-HCl-0.15 between 200 nm and 400 nm due to the presence of brookite in the as-prepared samples. Since the UV irradiation is utilized for the photocatalytic reaction, the lower light absorption may result in a lower photocatalytic activity.

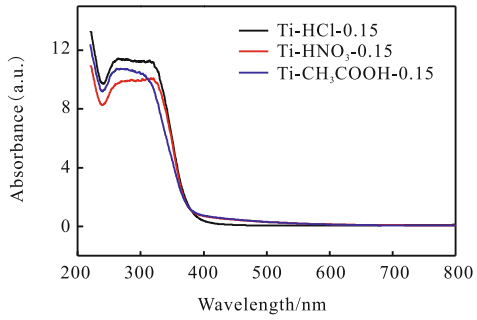

Fig. 5 UV-Vis diffuse reflectance spectra of Ti-HCl-0.15, Ti-HNO_3-0.15 and Ti-CH_3COOH-0.15

2.2 Photocatalytic activity of mixed-phase TiO_2 products

The photocatalytic activities of the resulting products were evaluated by the decolorization of rhodamine B (10 mg/L) in an aqueous solution under a 300 W UV lamp for 90 min. Fig. 6 shows that Ti-HCl-0.15 and Ti-HNO_3-0.15 have the highest photocatalytic activity in the samples prepared in HCl solution and HNO_3 solution, respectively. However, Ti-CH_3COOH-0.15 shows lower photocatalytic activity than Ti-CH_3COOH-1.5 and Ti-CH_3COOH-3.

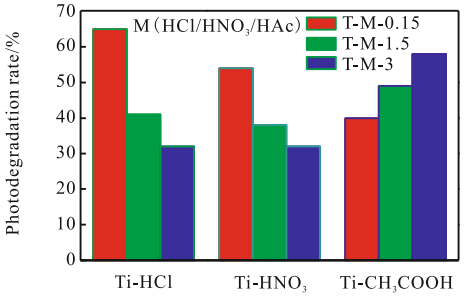

Fig. 6 Photodegradation of MB solution on Ti-HCl, Ti-HNO_3 and Ti-CH_3COOH

As shown in Fig. 6, the photocatalytic activity of Ti-HCl-0.15 (anatase/brookite mixed phase) is higher than those of Ti-HCl-1.5 and Ti-HCl-3, probably because anatase/brookite mixed phase has a synergistic effect on the enhancement of the photocatalytic activity due to a better electron transfer between two phases. It is the fact that the E_g values are various with the different rates of anatase/brookite in mixed phase. Ti-HCl-0.15 (85.2% anatase/14.8% brookite) and Ti-HNO_3-0.15 (80.1% ana-

tase/19.9% brookite) have higher E_g values than Ti-CH_3COOH-0.15 (98.9% anatase/1.1% brookite), as shown in Fig. 5, which can be attributed to the interfacial electron transfer from brookite into anatase, similar to those in Refs. [19] and [20].

The other reason why the photocatalytic activities of Ti-HCl-1.5 (43%) and Ti-HCl-3 (32%) are lower than that of Ti-HCl-0.15 can be attributed to the low surface area and low pore volume, as shown in Tab. 2. With the increase of HCl concentration, the photocatalytic activities of Ti-HCl-1.5 and Ti-HCl-3 decreased due to the increase of the content of rutile. This can be interpreted that although the presence of rutile is beneficial to the spatial charge separation of anatase/rutile mixed phase, the photocatalytic activity will be lost in a large amount of rutile. Therefore, there is an optimum amount of rutile phase in TiO_2[20]. The photocatalytic activity of Ti-HNO_3-0.15 is higher than those of Ti-HNO_3-1.5 and Ti-HNO_3-3 due to its larger surface area and anatase/brookite mixed phase. In addition, the photocatalytic activity of Ti-CH_3COOH-3 is higher than those of Ti-CH_3COOH-0.15 and Ti-CH_3COOH-1.5 due to its larger surface area and appropriate amount of rutile phase.

2.3 Mechanism

In this article, the fabrication process of the TiO_2 particles included the hydrolysis of titanium precursor, sol-gel transformation of the solution to xerogel, and further hydrothermal treatment in different acid solutions. The hydrolysis reaction led to the formation of original nuclei or TiO_2 basic units, while the condensation reaction led to the growth of network system of the original basic units[21]. The xerogel was found to contain some residues, mainly water, alcohols and/or residual alkoxy groups. Most organic compounds in xerogel powders could be removed at a relatively high temperature by hydrothermal treatment. Additionally, the product powders obtained were mixed phase of anatase, rutile and brookite with the hydrothermal treatment of TiO_2 xerogel in different acid solutions.

Some reports discussed the possible mechanism of the formation of anatase and rutile[22]. The basic units of octahedra TiO_6^{2-} in solution can join together to form oligomers which are the growth units leading to both anatase and rutile phases. The joining of the basic octahedral unit, if taking place at the opposite edges, would give a growth unit for the rutile phase. However, if it took place at the non-opposite edges, it would give a growth unit for the anatase phase, and possibly the brookite phase too. When TiO_2 xerogel was hydrothermally treated in an acid solution with a low concentration, the brookite phase appeared. With the increase of H^+ concentration, the basic octahedral unit taking place at the opposite edges would give a growth unit for the rutile phase, forming corner-sharing octahedral chains that are the characteristic of rutile phase, so the brookite phase disappeared. It can be observed in Fig. 1 (a) and (b) that the brookite phase decreases with the increase of concentration of HCl and HNO_3.

According to Ref. [23], in the hydrolysis of modified alkoxide precursors of the formula Ti(OR)-x(Ac)y, the chelating acetate was less hydrolyzable than the alkoxide (OR) groups and could only be removed by heating above 300 ℃. Doeuff *et al*[23] proposed the structures where acetate ligands are in bridging position (Fig. 7). The acetate, used as a chelating agent, hindered the growth of the chain along the opposite edges, and subsequently inhibited the formation of rutile phase. From Fig. 1 (c), the brookite phase only appeared in Ti-CH_3COOH-0.15, and the anatase phase was the major phase of Ti-CH_3COOH-0.15, Ti-CH_3COOH-1.5 and Ti-CH_3COOH-3. When the concentration of CH_3COOH is 3 mol/L, the formation of the rutile phase was encouraged in Ti-CH_3COOH-3 due to the high concentration of H^+.

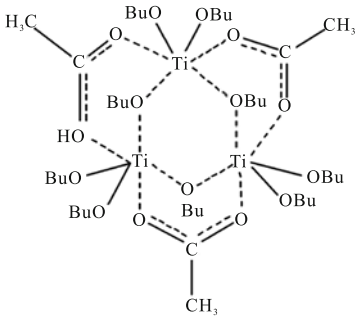

Fig. 7 Proposed structures for the product of the stoichiometric reaction (1 : 1 titanium to AcOH)

3 Conclusions

TiO_2 NPs were prepared via the hydrolysis of $Ti(OC_4H_9)_4$ to xerogel and further hydrothermal treatment in different acid solutions. Different acids exerted different surface interactions with TiO_2 precursor, and consequently formed different microstructures. When the catalyst was hydrothermally synthesized in a strong acid solution with a low concentration, the mixed phase of anatase/brookite could be obtained with small particle size, large surface area and mesoporous structure. How-

ever, when the catalyst was prepared in a weak acid solution with a high concentration, the mixed phase of anatase/rutile could be obtained with big particle size, large surface area and mesoporous structure. The catalyst obtained in the low-concentration hydrochloric acid solution (Ti-HCl-0.15) and high-concentration acetic solution (Ti-CH_3COOH-3) showed better photocatalytic activities than other catalysts probably due to the mixed phase and large surface area.

References

[1] Wong C L, Tan Y N, Mohamed A R *et al*. A review on the formation of titania nanotube photocatalysts by hydrothermal treatment[J]. *Journal of Environmental Management*, 2011, 92: 1669-1680.

[2] Tan Xin, Shi Ting, Yu Tao *et al*. High-reactive heterostructure TiO_2 /$SrTiO_3$ nanotube arrays and its photoelectrocatalytic performance[J]. *Journal of Tianjin University (Science and Technology)*, 2014, 47(11): 955-961(in Chinese).

[3] Xu Y, Fang X, Zhang Z *et al*. Formation of single-crystalline TiO_2 nanomaterials with controlled phase composition and morphology and the application in dye-sensitized solar cell[J]. *Applied Surface Science*, 2009, 255: 8743-8749.

[4] Zhang Q, Cao G. Nanostructured photoelectrodes for dye-sensitized solar cells[J]. *Nano Today*, 2011, 6: 91-109.

[5] Sotter E, Vilanova X, Llobet E *et al*. Thick film titania sensors for detecting traces of oxygen[J]. *Sensors and Actuators B: Chemical*, 2007, 127: 567-579.

[6] Chrystelle Salameh, Jean-Philipe Nogier, Franck Launay *et al*. Dispersion of colloidal TiO_2 nanoparticles on mesoporous materials targeting photocatalysis applications[J]. *Catalysis Today*, 2015, 257: 35-40.

[7] Lee J H, Kang M, Chong S J *et al*. The preparation of TiO_2 nanometer photocatalyst film by a hydrothermal method and its sterilization performance for *Giardia lamblia*[J]. *Water Research,* 2004, 38(3): 713-719.

[8] Leyva-Porras C, Toxqui-Teran A, O Vega-Becerra *et al*. Low-temperature synthesis and characterization of anatase TiO_2 nanoparticles by an acid assisted sol-gel method[J]. *Journal of Alloys and Compounds*, 2015, 647: 627-636.

[9] Huang D G, Liao S J, Quan S Q *et al*. Preparation of anatase F doped TiO_2 sol and its performance for photodegradation of formaldehyde[J]. *Journal of Material Science*, 2007, 42(19): 8193-8202.

[10] Khalil Kamal M S, El-Khatib Rafat M, Ali Tarek T *et al*. Titania nanoparticles by acidic peptization of xerogel formed by hydrolysis of titanium(IV) isopropoxide under atmospheric humidity conditions[J]. *Powder Technology*, 2013, 245: 156-162.

[11] Cheng Wei-Yun, Deka Juti Rani, Chiang Yi-Chun *et al*. One-step, surfactant-free hydrothermal method for syntheses of mesoporous TiO_2 nanoparticle aggregates and their applications in high efficiency dye-sensitized solar cells[J]. *Chemistry of Materials*, 2012, 24: 3255-3262.

[12] Wang Chao, Li Qin, Wang Ruoding . Synthesis and characterization of mesoporous TiO_2 with anatase wall[J]. *Materials Letters*, 2004, 58: 1424-1426.

[13] Zhang Q, Li Y, Ackerman E A *et al*. Visible light responsive iodine-doped TiO_2 for photocatalytic reduction of CO_2 to fuels[J]. *Applied Catalysis A*: *General*, 2011, 400(1/2): 195-202.

[14] Barrett E P, Joyner L G, Halenda P H *et al*. The determination of pore volume and area distributions in porous substances(I): Computations from nitrogen isotherms[J]. *Journal of the American Ceramic Society*, 1951, 73: 373-380.

[15] Gopal M, Chan W J M, De Jonghe L C *et al*. Room temperature synthesis of crystalline metal oxides[J]. *Journal of Material Science*, 1997, 32: 6001-6008.

[16] Rouquerol J, Rouquerol F, Sing K. *Adsorption by Powders and Porous Solids*: *Principles*, *Methodology*, *and Applications*[M]. Academic Press, San Diego, USA, 1999.

[17] Liu R, Ren Y, Shi Y *et al*. Controlled synthesis of ordered mesoporous C-TiO_2 nanocomposites with crystalline titania frameworks from organic-inorganic-amphiphilic coassembly[J]. *Chemistry of Material*, 2008, 20: 1140-1146.

[18] Wijesinghe W P S L, Mantilaka M M M G P G, Premalal E V A *et al*. Facile synthesis of both needle-like and spherical hydroxyapatite nanoparticles: Effect of synthetic temperature and calcination on morphology, crystallite size and crystallinity[J]. *Materials Science and Engineering C*, 2014, 42: 83-90.

[19] El-Sheikh Said M, Zhang Geshan, El-Hosainy Hamza M *et al*. High performance sulfur, nitrogen and carbon doped mesoporous anatase-brookite TiO_2 photocatalyst for the removal of microcystin-LR under visible light irradiations[J]. *Journal of Hazardous Materials*, 2014, 280: 723-733.

[20] Yan M, Chen F, Zhang J *et al*. Preparation of controllable crystalline titania and study on the photocatalytic properties[J]. *Journal of Physical Chemistry B*, 2005, 109(18): 8673-8678.

[21] Kumar S R, Suresh C, Vasudevan A K *et al*. Phase transformation in sol-gel titania containing silica[J]. *Material Letters*, 1999, 38: 161-166.

[22] Zheng Yanqing, Shi Erwei, Chen Zhizhan *et al*. Influence of solution concentration on the hydrothermal preparation of titania crystallites[J]. *Journal of Material Chemistry*, 2001, 11: 1547-1551.

[23] Doeuff S, Henry M, Sanchez C *et al*. Hydrolysis of titanium alkoxides: Modification of the molecular precursor by acetic acid[J]. *Journal of Non-Crystalline Solids*, 1987, 89: 206-216.

(Editor: Zhao Yang)